Using Flexible and Stretchable Surface Electromyography Electrode Array to Evaluate Congenital Muscular Torticollis in Children

Yuanheng Li, Jing Sun, Xin Qiu, Qingsong Li, Wei Wang, *Member, IEEE*, Shanshan Zhu, Jingjing Wei, Dianpeng Qi, Shixiong Chen, *Member, IEEE*, Shengping Tang, Zhu Xiong, Zhiyuan Liu, *Member, IEEE*, and Guanglin Li, *Senior Member, IEEE*

***Abstract*— Congenital Muscular Torticollis (CMT) is a neuromuscular disease in children, which leads to exacerbation of postural deformity and neck muscle dysfunction with age. Towards facilitating functional assessment of neuromuscular disease in children, topographic electromyography (EMG) maps enabled by flexible and stretchable surface EMG (sEMG) electrode arrays are used to evaluate the neck myoelectric activities in this study. Customed flexible and stretchable sEMG electrode arrays with 84 electrodes were utilized to record sEMG in all subjects during neck motion tasks. Clinical parameter assessments including the cervical range of motion (ROM), sonograms of the sternocleidomastoid (SCM), and corresponding histological analysis were also performed to evaluate the CMT. The muscle activation patterns of neck myoelectric activities between the CMT patients and the healthy subjects were asymmetric during different neck motion tasks. The CMT patients presented significantly lower values in spatial features of two-dimensional (2D) correlation coefficient, left/right energy ratio, and left/right energy difference ($p < 0.001$). The 2D correlation coefficient of activation patterns of neck rotation and extension in CMT patients significantly correlated with clinical parameter assessments ($p < 0.05$). The findings suggest that the spatial features of muscle activation patterns based on the sEMG electrode arrays can be utilized to evaluate the CMT. The flexible and stretchable sEMG electrode array is promising to facilitate the functional evaluation and treatment strategies for children with neuromuscular disease.**

***Index Terms*— Congenital muscular torticollis, sternocleidomastoid, muscle activation pattern, flexible and stretchable and electrode arrays.**

Manuscript received 31 October 2022; revised 6 March 2023; accepted 18 March 2023. Date of publication 1 May 2023; date of current version 1 June 2023. This work was supported in part by the National Key Research and Development Program of China under Grant 2021YFF0501601; in part by the National Natural Science Foundation of China under Grant 81927804, Grant 62103405, and Grant 62201559; in part by the Natural Science Foundation of Guangdong Province under Grant 2022A1515010169; in part by the Guangdong Basic and Applied Basic Research Foundation under Grant 2021A1515110879 and Grant 2023A1515011160; and in part by the Sanming Project of Medicine in Shenzhen under Grant SZSM202011012. *(Yuanheng Li, Jing Sun, and Xin Qiu contributed equally to this work.) (Corresponding authors: Shengping Tang; Zhu Xiong; Zhiyuan Liu.)*

This work involved human subjects or animals in its research. Approval of all ethical and experimental procedures and protocols was granted by the Institutional Review Board of Shenzhen Institutes of Advanced Technology, Chinese Academy of Sciences, under Approval No. SIAT-IRB-220115-H0582.

Yuanheng Li, Jing Sun, Qingsong Li, Wei Wang, Shanshan Zhu, Zhiyuan Liu, and Guanglin Li are with the CAS Key Laboratory of Human-Machine Intelligence-Synergy Systems and the SIAT Branch, Shenzhen Institute of Artificial Intelligence and Robotics for Society, Shenzhen 518055, China, and also with the Guangdong-Hong Kong-Macau Joint Laboratory of Human-Machine Intelligence-Synergy Systems, Shenzhen Institutes of Advanced Technology (SIAT), Chinese Academy of Sciences, Shenzhen 518055, China (e-mail: zy.liu1@siat.ac.cn).

Xin Qiu, Shengping Tang, and Zhu Xiong are with Shenzhen Children's Hospital, China Medical University, Shenzhen, Guangdong 518048, China (e-mail: tangshengping56@126.com; bamboobear@163.com).

Jingjing Wei and Shixiong Chen are with the Shenzhen Institutes of Advanced Technology, Chinese Academy of Sciences, SIAT Branch, Shenzhen 518055, China.

Dianpeng Qi is with the MIIT Key Laboratory of Critical Materials Technology for New Energy Conversion and Storage National and the Local Joint Engineering Laboratory for Synthesis, Transformation and Separation of Extreme Environmental Nutrients School of Chemistry and Chemical Engineering, Harbin 150001, China, and also with the Harbin Institute of Technology, Harbin 150001, China.

This article has supplementary downloadable material available at https://doi.org/10.1109/TNSRE.2023.3271650, provided by the authors.

Digital Object Identifier 10.1109/TNSRE.2023.3271650

I. Introduction

CONGENITAL Muscular Torticollis (CMT) is a disease that leads to multiple types of deformity of the body and progressive muscle dysfunction of the neck in the developmental stages of children with a reported incidence of 0.3% to 2% [1], [2], [3]. Its clinical symptoms are characterized by persistent lateral flexion and neck rotation towards the affected side due to the unilateral shortening of the sternocleidomastoid (SCM) [3]. Multiple etiologies [4], [5], [6] were found to be attributed to CMT, leading to the impairment of the developing SCM. The primary pathologic features [6] of CMT appear as excessive endomysial and perimysial fibrosis, adipocyte hyperplasia, and muscle atrophy, which are attributed to the muscle shortening of the SCM and restricted cervical range of motion. A variety of different muscular disorders presented with similar symptoms can be confused with CMT, while the etiologies might be ocular, orthopedic, neurologic, etc. Specifically, the dysfunction of SCM similar to CMT has not been found in these cases, such as the ocular torticollis caused by ocular muscle weakness [7], Sandifer's syndrome caused by gastroesophageal reflux [8], spasmodic torticollis (cervical dystonia) related to neuropathologic changes [9],

and self-limited case of benign paroxysmal torticollis [10]. Thereby differential diagnosis in those cases is easily confused and time-consuming, which may delay the treatment and lead to severe consequences [11], [12].

Among the clinical diagnosis methods, conventional B-mode ultrasonography (CBMU) is the most commonly used one to diagnose and evaluate torticollis, especially for phenotype with a palpable mass [13], [14]. It mainly evaluates the structure-related features on the sonogram, including muscle thickness, echogenicity, and transverse and longitudinal extents [15], [16]; and the correlation between these features and clinical assessments in CMT has been investigated accordingly [17], [18], [19]. In addition, sonoelastography also has been proved to effectively evaluate tissue stiffness within the selected zone of interest [20], which is the most commonly used type of elastography. The assessment outcomes of both methods are based on the pathological changes in muscle structure, where more qualitative rather than quantitative assessments are provided [21], [22]. Furthermore, evaluation of muscular functional changes cannot be achieved by those methods either. Clinical and neurophysiological studies have emphasized the value of sEMG in measuring cervical myoelectric activities with torticollis by using several paired sEMG electrodes or needle electrodes on the SCM [23], [24], [25]. To the best of our knowledge, few studies have investigated the extent of the affected SCM impact on neck muscle activities in children with CMT. Moreover, the application of commercial electrode arrays which do not have sufficient skin conformity is still limited by their configuration and material properties [26]. Therefore, the advanced sEMG technique [26], [27]would be a good solution, which can provide enriched spatial information on myoelectric activities.

In this study, a customed flexible and stretchable sEMG electrode array to evaluate neck muscle activation patterns during different neck motion tasks in children with CMT. The neck motion tasks selectively activate neck muscles in different neck areas. The topographic EMG maps provide spatial information about the affected side (if any) of interest without prior knowledge of neck anatomy. Spatial features of muscle activation patterns during neck motion tasks were analyzed using the two-dimensional (2D) correlation analysis, left/right energy ratio (LRER), and left/right energy difference (LRED), which were extracted from the sEMG signals. The difference in activation patterns between the CMT patients and the healthy subjects was compared via these features. Moreover, the topographic EMG map can help to identify the approximate location of lesion sites in the CMT patients. The proposed sEMG electrode array in this study may own the potential to evaluate the spatial distribution of neck muscle activities in children with CMT. Successful analysis may facilitate the functional assessment and treatment strategies for neuromuscular disease in children.

II. Materials and Methods

A. Subjects

Twenty subjects (ten males, ten females) were recruited for this study, including ten CMT patients (five males and five females) and ten healthy subjects (five males and five females). The mean ages of healthy subjects and CMT patients were 6.8 ± 1.2 and 6.5 ± 1.4, respectively. The lesion sites in CMT patients were distributed equally between the right and the left of SCM. Inclusion criteria include: (1) the patients were clinically confirmed with CMT; (2) the ultrasound examination showed that the muscle thickness on the affected side was significantly higher than that of the unaffected side; (3) the patients aged from 4 to 14 years old; (4) The patients recruited were on the condition that they were free of central or peripheral nerve diseases or other types of torticollis. All the patients with clinically confirmed CMT would receive the surgical treatment after all the data collection was complete. The experimental protocols were approved by the Institutional Review Board of Shenzhen Institutes of Advanced Technology, Chinese Academy of Sciences (IRB Number: SIAT-IRB-220115-H0582). All the subjects gave their consent for participation and publication of their data/photographs for scientific and educational purposes.

B. HD-sEMG Preparation and Measurements

Fabrication of customed flexible and stretchable sEMG electrode arrays: the conductive silver paste, which consists of elastomers and micro-sized silver flakes mixed in a volatile solvent, was directly printed on the back of the film dressing (*Tegaderm, style 4“ x 4-3/4”, 3M Health Care, St. Paul, MN, USA*) [28], [29] by using a specially designed template (Fig. 1.d). After the silver paste was dry, round holes with 3mm diameter were punched at the conductive silver paste and then filled with the conductive gel (*Wuhan Greentek Pty. Ltd, GT10*), which were composed of conductive contacts. And then, a new film dressing was attached for encapsulation and preparation. The prepared electrode arrays can be directly attached on the neck for EMG recording just by peeling off the encapsulated film dressing and connecting with the EMG recording system via a flexible printed circuit board (PCB). And then, the sEMG signals of whole muscle activities were obtained using a customed high-density biopotential signal collector and the sample rate was 1 kHz. (*NES-128B01, 128 channels, sample rate2KHz, Research Center for Neural Engineering, SIAT, CAS, China*). Up to 84 channels of EMG signals were simultaneously collected during neck motion tasks. The skin areas of the neck were carefully cleaned using alcohol cotton stickers to remove dry dermis and skin oils that may degrade the quality of the sEMG recordings. Then, the electrode arrays made up of 84 contacts were evenly aligned and placed on the anterior neck. Supraspinous of C7 was selected to place the reference electrode. The placement of the customed flexible and stretchable sEMG electrode arrays on the neck is shown in Fig. 1d.

In this study, six different neck motion tasks, including right neck rotation (RNR), left neck rotation (LNR), neck flexion (NF), neck extension (NE), left lateral flexion (LLF), and right lateral flexion (RLF), were introduced to the subjects. Following adaptive training, all the subjects were able to repeat this sequence of motion tasks in a nearly standardized manner. Then the cap with the gyro sensor adhered was put on the subject’s head to measure the ROM synchronously. After the

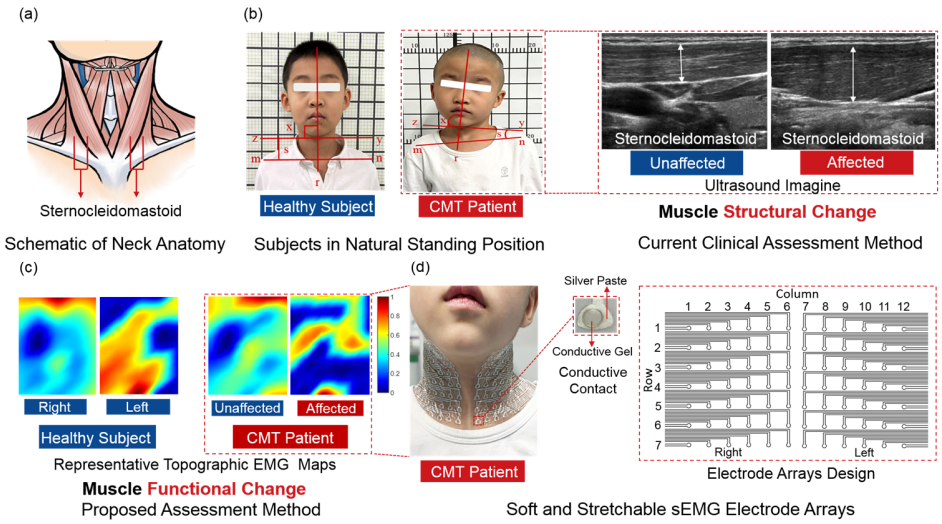

Fig. 1. The clinical parameter assessments and experimental setup of the proposed functional assessment on subjects. (a) Schematic of neck muscle anatomy; (b) The healthy subject and congenital muscular torticollis (CMT) patient are in their natural standing position. The angle x formed between zy and r and the angle s formed between zy and mn were used to evaluate the asymmetry between head and neck by digital photograph [30]; Ultrasound images show the sternocleidomastoid thickness on two sides in the CMT patient; (c) Typical topographic EMG maps of right neck rotation in a healthy subject and CMT patient; (d) Schematic diagram of neck muscles covered by the customed soft and stretchable surface electromyogram electrode arrays. Experimental photo with the electrode arrays placed on the neck of the CMT patient. Each array had six rows, seven columns, and 42 conductive contacts. The inter-electrode distance was 10 mm.

attachment of electrodes was accomplished, the subjects were instructed to complete the motion tasks with their maximum effort to ensure the activation level of neck muscles was the same. The subjects were required to sit upright and keep static during the trials. For each trial, the motion task lasted 5s and was repeated six times with an interval of 10s rest, and 30s movement was set to ensure the relaxation of subjects between the different trail.

C. Cervical Range of Motion Measurement

The cervical ROM of all the subjects in the position of sitting upright with shoulders stabilized and the head in their cervical neutral position(defined as 0°) was measured with a multi-stage gyro sensor (Wit-motion, WT901C485). In this study, all the ROM of different motion tasks were measured. The ROM of rotation for activating the affected side was defined as rotation toward the unaffected side, and the lateral flexion for activating the affected side was toward the affected side. The neutral Spine position was maintained through the whole process of the measurement that was recorded synchronously with the EMG signals recording

D. Ultrasound Examination

All the subjects underwent ultrasound examination (Vevo 6600; Visual Sonics, Toronto, ON, Canada) during the time of enrollment in the hospital, which was performed by two well-experienced radiologists. The procedure of ultrasound examination and image analysis was performed as previously described [13], and the anteroposterior diameter representing muscular thickness was measured for the structural analysis.

E. Signal Processing and Data Analysis

The raw sEMG signal filtering were performed with a fourth-order Butterworth band-pass filter (Cut-off frequencies

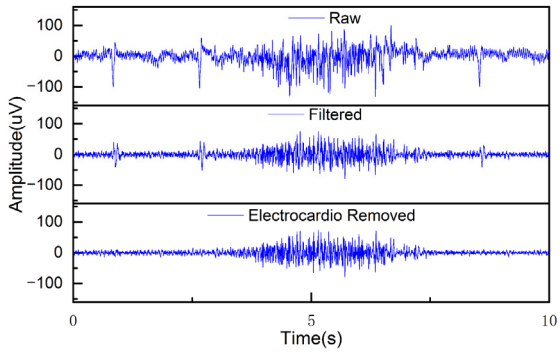

Fig. 2. Representative electromyographic signals following signal processing.

from 20 to 500Hz) and a 50 Hz notch filter by EEGLAB software (http://sccn.ucsd.edu/eeglab/). Additionally, electrocardiogram signals in the EMG data were removed using independent component analyses (Fig. 2). Procedures for electrode-skin impendence and signal and noise ratio analysis are described in the supplementary material.

Then root mean square (RMS) values of all channels for each trail were computed and normalized to the difference between the maximum and minimum RMS values for the trail. Then, the RMS values were organized as a matric RMS_{mat} according to the layout of electrode arrays (for examples see equations (1)).

$$RMS_{mat} = \begin{bmatrix} RMS_{mat1,1} & \cdots & RMS_{mat1,12} \\ \vdots & \ddots & \vdots \\ RMS_{mat7,1} & \cdots & RMS_{mat7,12} \end{bmatrix}_{7X12} \quad (1)$$

The spatial distribution of activated muscles was presented by topographic EMG maps using cubic spline interpolation.

The maps enable researchers to observe the position and outline of activated neck muscles during the neck mJtion tasks. The maps were constructed by converting the amplitude value of normalized RMS into the corresponding color.

The neck muscle activation patterns during different motion tasks on the topographic EMG maps was evaluated using the following metrics (Correlation Coefficient ρ, LRER and LRED equations (2-4)).

$$p = \frac{\sum_m \sum_n (L_{m,n} - \overline{L})(R_{m,n} - \overline{R})}{\sqrt{(\sum_m \sum_n (L_{m,n} - L)^2)(\sum_m \sum_n (R_{m,n} - \overline{R})^2)}} \tag{2}$$

$$LRER = \frac{\sum_m \sum_n (RMS_{mat,left})_{m,n}}{\sum_m \sum_n (RMS_{mat,right})_{m,n}} \tag{3}$$

$$LRED = \frac{\sum_m \sum_n (RMS_{mat,left} - RMS_{mat,right})_{m,n}}{\sum_m \sum_n (RMS_{mat,N})_{m,n} \div 2} \text{x}100\% \tag{4}$$

To evaluate the 2D correlation of activation patterns during neck rotation and lateral flexion, the RMS_{mat} of left neck rotation and lateral flexion were flip over around axis of the first column, respectively. (for examples see equations (5, 6)). In terms of neck flexion and extension, the RMS_{mat} of left side of neck flexion and extension were also mirror-transferred (for examples see equations (7, 8)). Spatial features of the 2D correlation coefficient (corr2), LRER, and LRED [31] were calculated to quantitatively evaluate the distribution of neck muscle activities during motion tasks. The matrices (L and R) are compared, such as $L_{m,n}$ and $R_{m,n}$, and $\overline{L}$ and $\overline{R}$ are the mean values of L and R, respectively. $RMS_{mat,N}$ is the summation of the RMS values from the left and right electrode arrays, correspondingly. (m,n) represents the spatial position of a channel in the matrix. The comparison of corr2 between two sides among different motion tasks was performed separately. And the comparison between the healthy subjects and CMT patients was made during motion tasks. The statistical analysis was performed further to investigate the differences between healthy subjects and CMT patients.

$$RMS_{mat,\text{ right neck rotation}} = \begin{bmatrix} RMS_{mat1,1} & \cdots & RMS_{mat1,12} \\ \vdots & \ddots & \vdots \\ RMS_{mat7,1} & \cdots & RMS_{mat7,12} \end{bmatrix} \tag{5}$$

$$RMS_{mat,\text{ left neck rotation}} = \begin{bmatrix} RMS_{mat1,12} & \cdots & RMS_{mat1,1} \\ \vdots & \ddots & \vdots \\ RMS_{mat7,12} & \cdots & RMS_{mat7,1} \end{bmatrix} \tag{6}$$

$$RMS_{mat,\text{ right}} = \begin{bmatrix} RMS_{mat1,1} & \cdots & RMS_{mat1,6} \\ \vdots & \ddots & \vdots \\ RMS_{mat7,1} & \cdots & RMS_{mat7,6} \end{bmatrix} \tag{7}$$

$$RMS_{mat,\text{ left}} = \begin{bmatrix} RM_{mat12,1} & \cdots & RMS_{mat1,7} \\ \vdots & \ddots & \vdots \\ RS_{mat12,7} & \cdots & RMS_{mat7,7} \end{bmatrix} \tag{8}$$

F. Statistical Analysis

Statistical analysis was performed using SPSS (*IBM, Armonk, NY, USA*). The comparison of the spatial features of the topographic EMG map and the cervical ROM between healthy subjects and CMT patients during different motion tasks was evaluated by performing non-paired two-sample t-tests. Paired t-tests were used to analyze the differences in sonogram parameters between the affected side and the unaffected side in patients with CMT. The multivariate correlation analysis based on Pearson's correlation coefficient was calculated among the metrics of sEMG and clinical parameter assessments using Origin software (Origin 2021, Microcal Software Inc., Northampton, MA, USA) for statistical analysis. P values less than 0.05 were taken as the threshold of statistical significance.

III. Results

A. Muscle Activation Patterns Based on HD-sEMG

The results showed that the muscle activation patterns of neck muscles were distinct during different neck motion tasks and the activated muscles on the topographic EMG map were presented as the high-intensity zones. Fig. 3a shows the schematic of six different motion tasks. The muscle activation patterns based on sEMG between the healthy subjects and the CMT patients were not similar during the motion tasks. (Fig. 3b and 2c). During neck rotations, the location of high-intensity zones on the topographic EMG maps was mainly around the bottom of the map in the healthy subjects, which was opposed to the direction of neck rotation. For the CMT patients, the high-intensity zone on the EMG map mainly concentrated on the top zone of the map during the right rotation. During the left rotation, the area of the high-intensity zone on the EMG map in the CMT patients was smaller than that of the healthy subject. During lateral flexion, the location of the high-intensity zone on the EMG map was mainly concentrated at the bottom in the healthy subjects, which was consistent with the direction of the motion. For the CMT patients, the high-intensity zone was mainly concentrated around the top left corner on the unaffected side during the right lateral flexion. During the left lateral flexion, the area of the high-intensity zone of the EMG map was larger than that of the healthy subject.

As shown in the topographic EMG map Fig. 3c, the high-intensity zones of the EMG map were mainly concentrated on the midline and lateral sides in the healthy subjects during neck flexion. For the CMT patients, the spatial absence around the midline of the EMG map on the affected side was found compared with the healthy subject (Fig. 3b). During neck extension, the high-intensity zones of the EMG map were at the bottom of both sides in the healthy subjects (Fig. 3c). For the CMT patients, the area of the high-intensity

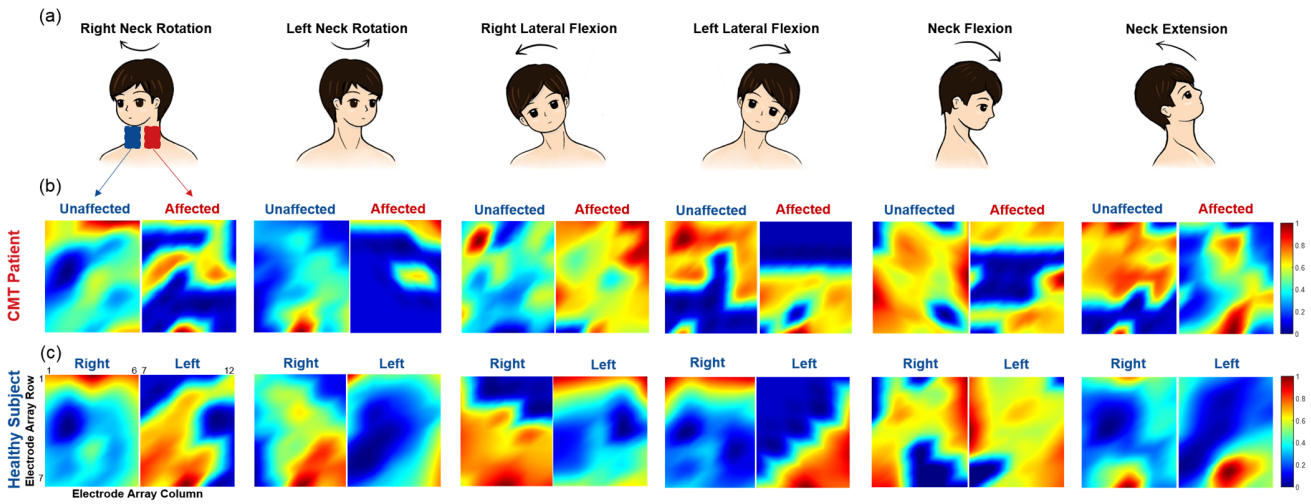

Fig. 3. Representative topographic EMG map of the healthy and the CMT subjects during six different neck motion tasks. (a) Schematic diagram of six neck motion tasks. The neck motion tasks correspond to the topographic EMG maps in (b) and (c); (b) The topographic EMG map of a CMT patient during six different neck motion tasks. The 'Right' and 'Left' is equivalent to 'Unaffected' and 'Affected' in the CMT patients; (c) The topographic EMG map of a healthy subject during six different neck motion tasks. 'Right' and 'Left' on the EMG map is equivalent to the sides of the healthy subjects.

zones of the EMG map was larger than that of the healthy subject (Fig. 3b). There was no apparent high-intensity zone on the EMG maps during rest in all subjects, thereby spatial characteristics of the EMG maps were not analyzed in the following sections. These results showed that the distribution of high-intensity zones in the CMT patients was not similar to that of the healthy subjects during neck motion tasks.

Fig. 4a shows the mean corr2 values in the healthy subjects and in the CMT patients. For the healthy subjects, the mean corr2 values were close to the value 1, indicating the similar muscle activation patterns of the two sides in all motion tasks. By contrast, the mean corr2 values were much lower than the value 1 for the CMT patients, indicating the dissimilar muscle activation patterns of the affected side and unaffected during different motion tasks. In addition, the mean corr2 values in healthy subjects were higher than those in the CMT patients ($p < 0.001$). Then the similarity between the two sides of the neck in all subjects was further analyzed via the LRER and LRED parameters. Fig. 4b and 4c show that, for the healthy subjects, all the mean values of LRER and LRED were close to 1 and 0, respectively. While for the CMT patients, such mean values of LRER were lower than 0.8 and the mean values of LRED were close to -1. Moreover, the mean values of both LRER and LRED in the healthy subjects were higher than those in the CMT patients ($p < 0.001$).

B. Cervical Range of Motion Analysis

Fig.5 shows that only the ROM of lateral flexion in the CMT patients was lower than that in the healthy subjects ($p < 0.001$ and $p < 0.01$, respectively). The differences of ROM in the other four motion tasks between the healthy subjects and the CMT patients were not statistically significant ($p > 0.05$).

C. Ultrasound Examination Analysis

Fig. 6 shows the selected regions of interest were manually selected on sonograms. Table I illustrates the mean values of sonogram parameters in CMT patients. The brightness, min Feret's diameter, and muscle thickness on the affected side were significantly greater than those of the unaffected side ($P < 0.05$).

TABLE I
MEAN VALUES OF ROM AND SONOGRAM PARAMETERS IN CMT PATIENTS

Sonogram Parameters	AS	UAS	AS/UAS Ratio
Area, cm^2	2.03±0.93	1.86±0.47	1.02±0.27
Brightness, %	27.03±4.83	22.49±4.51	1.23±0.19
Max Feret's diameter, cm	3.53±0.84	3.96±0.88	0.92±0.10
Min Feret's diameter, cm	0.81±0.26	0.63±0.14	1.29±0.18
Width, cm	3.50±0.84	3.91±0.88	0.93±0.11
Thickness, cm	7.40±1.79	5.18±1.31	1.44±0.25

Note: ROM: range of motion; AS: affected side; UAS: unaffected

D. Correlation Between the Metrics of sEMG and Clinical Parameter Assessments

The correlation analysis among the three metrics (corr2, LRER and LRED) of sEMG and clinical parameters is shown in Fig. 7. These clinical parameter assessments mainly focused on the structural and pathological changes in the SCM (except the ROM measurement). All the metrics of the motion tasks that mainly recruited SCM showed significant correlation with several clinical parameters. In terms of neck rotation, there was a significant correlation between corr2 and min feret's diameter and muscle thickness, respectively (Fig. 7a). For the LRER and LRED, Fig. 7b and 7c showe significant correlations between the neck rotation and max feret's diameter as well as width, respectively. In terms of neck flexion, the metrics of corr2 and LRED showed a significant correlation between area and thickness. In terms of neck extension, both the metrics of

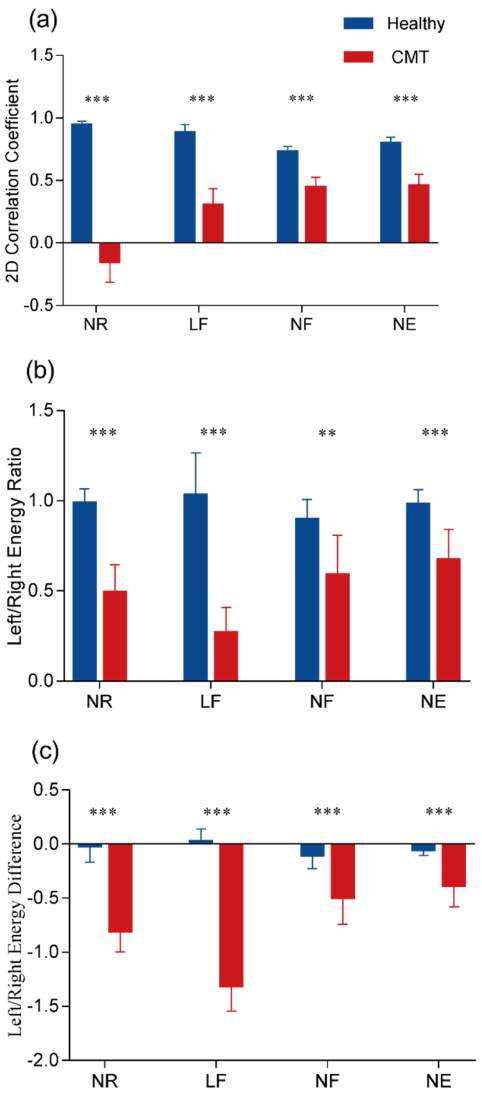

Fig. 4. Comparison of the spatial features between the healthy subjects and the CMT patients. (a): Comparison of the mean corr2 values between the healthy subjects and the CMT patients during different neck motion tasks; (b) and (c): Comparison of left/right energy ratio (LRER) and left/right energy difference (LRED) during different motion tasks to evaluate the symmetry of the two sides. Error bars represented the standard deviation between subjects (*p $<$ 0.05, ** p $<$ 0.01, *** p $<$ 0.001).

corr2 and LRER significantly correlated with brightness. For the correlation analysis among clinical parameters, there was a significant correlation among width, max feret's diameter, thickness, and lateral flexion of AS/UAS Ratio of ROM, respectively. These results indicated that the three metrics of some motion tasks owns the potential to evaluate the condition of the CMT.

IV. Discussion

In some research and clinical practices, the high-intensity spatial features enable researchers to acquire sufficient information on muscle activities as well as the central and peripheral characteristics of neuromuscular disease [31], [32]. In this study, we successfully recorded the sEMG signals and evaluated the neck muscle activation patterns in all subjects through the customed flexible and stretchable electrode arrays, which

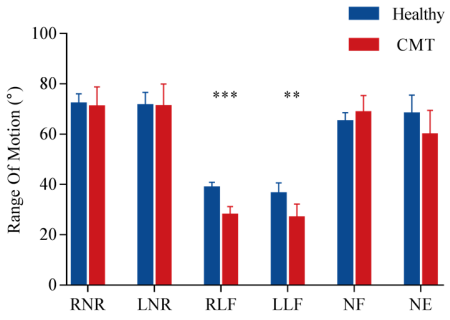

Fig. 5. The comparison of ROM between the healthy subjects and the CMT patients during six motion tasks. Right neck rotation (RNR), left neck rotation (LNR), neck flexion (NF), neck extension (NE), left lateral flexion (LLF), and right lateral flexion (RLF). Error bars represented the standard deviation between subjects (* p $<$ 0.05, ** p $<$ 0.01, *** p $<$ 0.001).

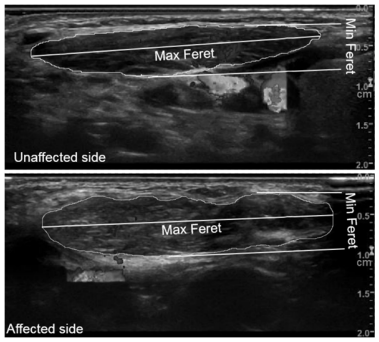

Fig. 6. Representative transverse sonograms of sternocleidomastoid muscle with the region of interest in the patients.

provided spatial information on neck muscle activities for clinical research.

A. Muscle Activation Pattern During Different Motion Tasks

The lesion of SCM in the CMT patients led to a different extent of changes in muscle activation pattern compared with that in the healthy subjects. For the CMT patients, the muscle activation patterns mainly presented the following characteristics during neck motion tasks: (i) the spatial distribution of the high-intensity zones on the topographic EMG maps was asymmetrical between the two sides; (ii) the spatial features extracted from the topographic EMG maps were significantly lower than those in the healthy subjects.

Furthermore, the asymmetry of muscle activation patterns in CMT patients may be attributed to the following reasons. (a) In terms of the right neck rotation, although the spatial absence around the lower segment of SCM was found on the EMG map, the ROM showed no significant difference between the CMT patients and the healthy subjects. It indicated that the ROM of this motion was not restricted anymore in this age group (6.5 $\pm$ 1.4). In addition, the neck rotation mainly recruited SCM as the antagonist muscle, and the actuating of this motion was mainly dominated by the posterior neck muscle groups such as the splenius capitis. Based on this, we suspected that the coexistence of insufficient muscle strength of agonist muscle and pathological changes in CMT may contribute to the neck rotation limitation [33], [34] for younger patients. Furthermore, the recovery of the neck

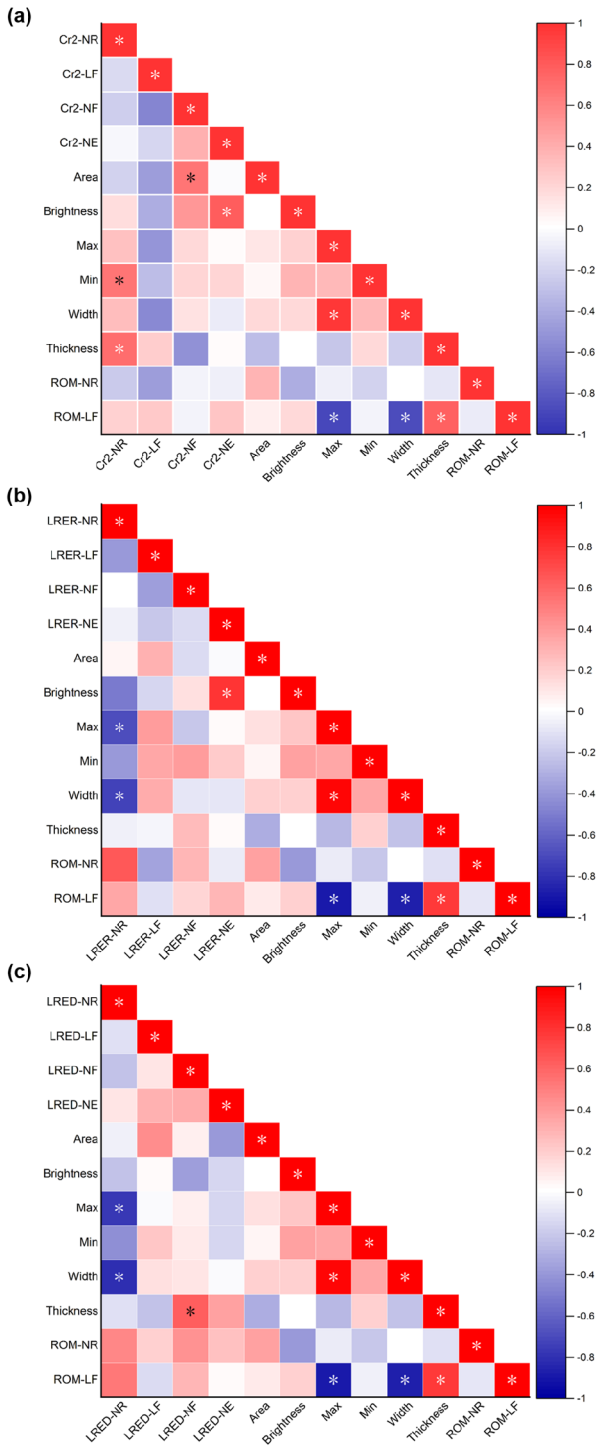

Fig. 7. The correlation matrix of the three metrics of sEMG and clinical parameters. (a): the correlation coefficients between the two dimensional correlation coefficient (corr2) and clinical parameter assessments; (b): the correlation coefficients between the left/right energy ratio (LRER) and clinical parameter assessments; (c): the correlation coefficients between the left/right energy difference (LRED) and clinical parameter assessments. Cr2 (corr2), AS/US Ratio of ROM (ROM), neck rotation (NR), lateral flexion (LF), neck flexion (NF), and neck extension (NE), max feret's diameter (Max), and min feret's diameter (Min). Note: The asterisk indicates the p-value less than 0.05.

rotation may be associated with the growth and development of dominated muscle (agonist muscle), and the spatial absence on the EMG map may be the lesion site of CMT. Regarding the left neck rotation, the smaller area of the high-intensity zone around the SCM was found on the EMG map compared with that in the healthy subjects. It implies that only partial muscle of the SCM was activated in this motion. Moreover, the clinical symptoms of CMT are characterized by neck rotation and lateral flexion, indicating the patients have suffered from persistent constantly unilateral passive stretching [4] for a long time. Therefore, we suspected that the muscle groups might engage in a more 'efficient' way when the direction of the motion was consistent with the location of the lesion site. (b) In terms of right lateral flexion, different locations of high-intensity zones in CMT patients indicated the SCM and the scalenus muscle were not fully activated compared with the healthy subjects. In addition, the mean value of LRED during lateral flexion in the CMT patients was -1.31 ± 0.22, indicating the summation of the RMS value on the unaffected side was greater than that on the affected side. These results indicated that partial SCM or some other muscles contributed to this motion. Moreover, when the patients were performing this motion (head laterally flexed to the unaffected side), first, the muscles on the unaffected side needed to overcome the traction due to the shortened SCM on the affected side. Thereby we suggest that the high-intensity zone around the upper segment of the SCM may mainly contribute to this motion in CMT patients. (c) In terms of neck flexion, the spatial absence of the high-intensity zone around the infrahyoid muscle was found on the EMG map, indicating the muscle was not recruited in this motion{O'Leary, 2007 #216}. As the lesioned SCM led to the constantly passive stretching on the affected side, the patients may flex their heads towards the affected side unconsciously during this motion. No significant difference in ROM was found between the CMT patients and the healthy subjects ($p > 0.05$). Therefore, we suspect that the patients may have developed a different muscle control strategy in this motion. (d) In terms of the neck extension, the asymmetrical activation pattern was attributed to the unequal muscle length on two sides in the CMT patients. During this motion, the agonist muscles from the posterior neck such as spinalis capitis also needed to overcome the traction due to the shortened SCM on the affected side. It is worth noting that the high-intensity zone on the affected around the lower segment of the SCM was similar to that in the healthy subjects and the larger area of the high-intensity zone on the unaffected side was found in the CMT patients, but the mean values of LRER and LRED were lower than those in the healthy subjects ($p < 0.001$). Such phenomenon was also found in the left lateral flexion, indicating the strength of the activated muscles was compromised due to pathological changes [35] in CMT. For the CMT patients, the functional changes were mainly characterized by the asymmetrical activation patterns, which presented as spatial absence or smaller area of the high-intensity zone around the activated muscle during neck motion tasks.

B. The Correlation Between Spatial Features of the Topographic EMG Map and Clinical Parameters

The spatial features that were extracted from the topographic EMG map quantified the similarity of activation

patterns between the patients and healthy subjects. The clinical parameters mainly confirmed the structural and pathological changes in CMT patients, which were significantly correlated with CMT in clinical research [19], [34]. The multivariate correlation analysis among the three metrics (corr2, LRER and LRED) of sEMG and the clinical parameter assessments was utilized to further explore the connection among the functional, structural, and pathological changes. Significant correlation was found among the clinical parameters, which was consistent with the previous researches [19], [20]. In addition, the clinical parameters mainly concentrate on evaluating the changes in SCM, which is the only lesioned muscle reported in the previous studies of CMT [6], [18], [19]. In this study, the results revealed that the three metrics in patients during neck rotation, neck flexion, and neck extension were significantly correlated with some clinical parameter assessments. Moreover, although the clinical symptoms are characterized by persistent lateral flexion and neck rotation [3], no significant correlation was found among the metrics of sEMG and clinical parameters. Thereby we suggest that the three metrics of sEMG in neck rotation, neck flexion, and neck extension may be more suitable than other motion tasks to evaluate the condition of CMT quantitatively. In this study, we found that the high-intensity zones on the EMG map were concentrated around multiple muscles during lateral flexion. Although no significant correlation among the three metrics and clinical parameter assessments was found in these motions, the asymmetry of muscle activation patterns in the CMT patients does exist in lateral flexion. Considering the posterior neck muscles were not analyzed in this study, analysis of the muscle synergy strategies of the anterior and posterior neck muscle groups may further reveal the neuromuscular control strategies [32] of the CMT patients.

In addition, previous studies suggested that neck motor abnormalities in CMT patients mainly showed the lateral flexion and neck rotation limitation [33], [34], but the abnormal ROM in neck rotation cannot be found in this study. Therefore, we suggest that the utilization of ROM in neck rotation to evaluate the severity of CMT may not be appropriate for CMT patients in this age group anymore. No statistical difference was found in the ROM of lateral flexion between the left lateral flexion and right lateral flexion in the CMT patients ($p > 0.05$) but the ROM in CMT patients was lower than that in the healthy subjects, indicating the ROM in lateral flexion mainly characterized the neck motor abnormalities instead of measuring the severity of the CMT. This may explain why no significant correlation was found among the three metrics of sEMG and the cervical ROM.

C. Limitations and Future Direction of Study

Despite the good findings, this study had several limitations. This research mainly involves a total of ten healthy subjects (five male and five female) and ten CMT patients (five male and five female). Statistical analyses were conducted, and the results provided significant differences for the conclusions. Therefore, although the sample size is not large, we think this study provided representative observations, which is helpful for evaluating the neck muscle activation pattern of CMT patients. sEMG signals of posterior neck muscles were not collected in this study, which was recruited as agonist muscles in some motion tasks. Thereby future research would focus on CMT with simultaneous collection of the anterior and posterior neck muscles motion to analyze the muscle synergies, for further investigating the neuromuscular control strategy and characterizing the progress of CMT.

V. Conclusion

This pilot study investigated the neck muscle activation patterns of myoelectric activities in children with CMT during different neck motion tasks. The differences of functional changes between the CMT patients and healthy subjects were evaluated using spatial features: corr2, LRER, and LRED. The results reveal that the muscle activation patterns were not similar between the two sides in the CMT patients. The spatial features between the CMT patients and that in the healthy subjects were significantly different. Moreover, the correlation between the spatial feature and the clinical parameter assessments was analyzed in this study. The muscle activation patterns of neck rotation and extension were suitable for functional analysis, which had a significant correlation with multiple clinical parameter assessments. The findings of this study indicate that the neck muscle activation patterns own the potential to evaluate and further provide treatment strategies for neuromuscular diseases in children such as CMT. The proposed advanced sEMG technique based on customed flexible and stretchable sEMG electrode arrays can provide information on neck muscle activities at the spatial level and is promising to facilitate the functional evaluation for neuromuscular diseases in children.

References

[1] M.-M. Chen, H.-C. Chang, C.-F. Hsieh, M.-F. Yen, and T. H.-H. Chen, "Predictive model for congenital muscular torticollis: Analysis of 1021 infants with sonography," *Arch. Phys. Med. Rehabil.*, vol. 86, no. 11, pp. 2199–2203, Nov. 2005.

[2] H. E. I. Aarnivala, A. M. Valkama, and P. M. Pirttiniemi, "Cranial shape, size and cervical motion in normal newborns," *Early Hum. Develop.*, vol. 90, no. 8, pp. 425–430, Aug. 2014.

[3] L. Stellwagen, E. Hubbard, C. Chambers, and K. L. Jones, "Torticollis, facial asymmetry and plagiocephaly in normal newborns," *Arch. Disease Childhood*, vol. 93, no. 10, pp. 827–831, Oct. 2008.

[4] J. R. Davids, D. R. Wenger, and S. J. Mubarak, "Congenital muscular torticollis: Sequela of intrauterine or perinatal compartment syndrome," *J. Pediatric Orthopedics*, vol. 13, no. 2, p. 141, 1993.

[5] S. J. Lee et al., "Comparison of clinical severity of congenital muscular torticollis based on the method of child birth," *Ann. Rehabil. Med.*, vol. 35, no. 5, p. 641, 2011.

[6] H.-X. Chen et al., "Fibrosis, adipogenesis, and muscle atrophy in congenital muscular torticollis," *Medicine*, vol. 93, no. 23, p. e138, 2014.

[7] M. R. Akbari, M. Khorrami Nejad, F. Askarizadeh, F. F. Pour, M. R. Pazooki, and M. R. Moeinitabar, "Facial asymmetry in ocular torticollis," *J. Current Ophthalmol.*, vol. 27, nos. 1–2, pp. 4–11, Mar. 2015.

[8] T. A. Angerpointner, "Sandifer syndromea multidisciplinary diagnostic and therapeutic challenge, 203–206," *J. Pediatric Surg.*, vol. 43, no. 1, p. 253, 2008.

[9] J. Jankovic, S. Leder, D. Warner, and K. Schwartz, "Cervical dystonia: Clinical findings and associated movement disorders," *Neurology*, vol. 41, no. 7, p. 1088, Jul. 1991.

[10] N. P. Rosman, L. M. Douglass, U. M. Sharif, and J. Paolini, "The neurology of benign paroxysmal torticollis of infancy: Report of 10 new cases and review of the literature," *J. Child Neurol.*, vol. 24, no. 2, pp. 155–160, Feb. 2009.

[11] N. Seyhan, L. Jasharllari, M. Keskin, and N. Savacı, "Efficacy of bipolar release in neglected congenital muscular torticollis patients," *Musculoskeletal Surg.*, vol. 96, no. 1, pp. 55–57, Jun. 2012.

[12] S. Patwardhan, A. K. Shyam, P. Sancheti, P. Arora, T. Nagda, and P. Naik, "Adult presentation of congenital muscular torticollis: A series of 12 patients treated with a bipolar release of sternocleidomastoid and Z-lengthening," *J. Bone Joint Surg. Brit. Volume*, vol. 93, no. 6, pp. 828–832, 2011.

[13] J. C. Y. Cheng, S. P. Tang, T. M. K. Chen, M. W. N. Wong, and E. M. C. Wong, "The clinical presentation and outcome of treatment of congenital muscular torticollis in infants—A study of 1,086 cases," *J. Pediatric Surg.*, vol. 35, no. 7, pp. 1091–1096, Jul. 2000.

[14] T. T. Do, "Congenital muscular torticollis: Current concepts and review of treatment," *Current Opinion Pediatrics*, vol. 18, no. 1, p. 26, 2006.

[15] T. C. Hsu, C. L. Wang, M. K. Wong, K. H. Hsu, F. T. Tang, and H. T. Chen, "Correlation of clinical and ultrasonographic features in congenital muscular torticollis," *Arch. Phys. Med. Rehabil.*, vol. 80, no. 6, pp. 637–641, 1999.

[16] J. D. Han, S. H. Kim, S. J. Lee, M. C. Park, and S. Y. Yim, "The thickness of the sternocleidomastoid muscle as a prognostic factor for congenital muscular torticollis," *Ann. Rehabil. Med.*, vol. 35, no. 3, pp. 361–368, 2011.

[17] Y.-T. Lee et al., "Clinical features and outcome of physiotherapy in early presenting congenital muscular torticollis with severe fibrosis on ultrasonography: A prospective study," *J. Pediatric Surg.*, vol. 46, no. 8, pp. 1526–1531, Aug. 2011.

[18] J. C.-Y. Cheng, C. Metreweli, T. M.-K. Chen, and S.-P. Tang, "Correlation of ultrasonographic imaging of congenital muscular torticollis with clinical assessment in infants," *Ultrasound Med. Biol.*, vol. 26, no. 8, pp. 1237–1241, Oct. 2000.

[19] C.-H. Lin, H.-C. Hsu, Y.-J. Hou, K.-H. Chen, S.-H. Lai, and W.-M. Chang, "Relationship between sonography of sternocleidomastoid muscle and cervical passive range of motion in infants with congenital muscular torticollis," *Biomed. J.*, vol. 41, no. 6, pp. 369–375, Dec. 2018.

[20] S.-Y. Lee et al., "Value of adding sonoelastography to conventional ultrasound in patients with congenital muscular torticollis," *Pediatric Radiol.*, vol. 43, no. 12, pp. 1566–1572, Dec. 2013.

[21] D. R. Kwon and G. Y. Park, "Diagnostic value of real-time sonoelastography in congenital muscular torticollis," *J. Ultrasound Med.*, vol. 31, no. 5, pp. 721–727, May 2012.

[22] G. Y. Park, D. R. Kwon, and D. G. Kwon, "Shear wave sonoelastography in infants with congenital muscular torticollis," *Medicine*, vol. 97, no. 6, p. e9818, 2018.

[23] M. A. J. Tijssen, "Frequency analysis of EMG activity in patients with idiopathic torticollis," *Brain*, vol. 123, no. 4, pp. 677–686, Apr. 2000.

[24] L. Werdelin et al., "The utility of EMG interference pattern analysis in botulinum toxin treatment of torticollis: A randomised, controlled and blinded study," *Clin. Neurophysiol.*, vol. 122, no. 11, pp. 2305–2309, Nov. 2011.

[25] C. Marin, M. J. Martí, E. Tolosa, R. Alvarez, L. Montserrat, and J. Santamaria, "Muscle activity changes in spasmodic torticollis after botulinum toxin treatment," *Eur. J. Neurol.*, vol. 1, no. 3, pp. 243–247, Jan. 1995.

[26] S. Chandra et al., "Performance evaluation of a wearable tattoo electrode suitable for high-resolution surface electromyogram recording," *IEEE Trans. Biomed. Eng.*, vol. 68, no. 4, pp. 1389–1398, Apr. 2021.

[27] B. B. Murphy et al., "A gel-free $Ti_3C_2T_x$-based electrode array for high-density, high-resolution surface electromyography," *Adv. Mater. Technol.*, vol. 5, no. 8, 2020, Art. no. 2000325.

[28] T. Ha et al., "Soft bioelectronics: A chest-laminated ultrathin and stretchable E-Tattoo for the measurement of electrocardiogram, seismocardiogram, and cardiac time intervals (Adv. Sci. 14/2019)," *Adv. Sci.*, vol. 6, no. 14, Jul. 2019, Art. no. 1970082.

[29] X. Zhao et al., "A fully flexible intelligent thermal touch panel based on intrinsically plastic Ag_2S semiconductor," *Adv. Mater.*, vol. 34, no. 13, Apr. 2022, Art. no. 2107479.

[30] S. Karacay, S. Arda, U. Alici, and B. Tokar, "Para-axillary subcutaneous endoscopic approach in torticollis: Tips and tricks in the surgical technique," *Eur. J. Pediatric Surg.*, vol. 25, no. 2, pp. 165–170, Dec. 2013.

[31] M. Zhu et al., "Evaluation of normal swallowing functions by using dynamic high-density surface electromyography maps," *Biomed. Eng. OnLine*, vol. 16, no. 1, p. 133, Dec. 2017.

[32] W. Wang et al., "Synergy analysis of back muscle activities in patients with adolescent idiopathic scoliosis based on high-density electromyogram," *IEEE Trans. Biomed. Eng.*, vol. 69, no. 6, pp. 2006–2017, Jun. 2022, doi: 10.1109/tbme.2021.3133583.

[33] J. C. Y. Cheng, M. W. N. Wong, S. P. Tang, T. M. K. Chen, S. L. F. Shum, and E. M. C. Wong, "Clinical determinants of the outcome of manual stretching in the treatment of congenital muscular torticollis in infants," *J. Bone Joint Surg.-Amer. Volume*, vol. 83, no. 5, pp. 679–687, May 2001.

[34] J.-Y. Lee et al., "The cervical range of motion as a factor affecting outcome in patients with congenital muscular torticollis," *Ann. Rehabil. Med.*, vol. 37, no. 2, p. 183, 2013.

[35] M. Du, X. Yan, J. F. Tong, J. Zhao, and M. J. Zhu, "Maternal obesity, inflammation, and fetal skeletal muscle development," *Biol. Reproduction*, vol. 82, no. 1, pp. 4–12, Jan. 2010.